UNIVERSITAT POLITÈCNICA DE VALÈNCIA

UNIVERSITY OF BRISTOL

AERODYNAMIC PERFORMANCE INVESTIGATION OF THE USE OF SLOTTED AIRFOILS AS A PASSIVE BOUNDARY LAYER CONTROL METHOD FOR ROTORCRAFT APPLICATIONS

Bachelor's thesis

AEROSPACE ENGINEERING

AUTHOR: CARLA CONESA FUENTES

Tutor: Dr MARK GILBERSTON

External cotutor: XANDRA MARGOT

ACADEMIC YEAR: 2021-2022

Aerodynamic performance investigation of the use of slotted airfoils as a passive boundary layer control method for wind turbine applications

Carla Conesa Fuentes

Department of Aerospace Engineering, University of Bristol, Queen's Building, University Walk, Bristol. BS8 1TR. UK.

ABSTRACT

In this research project, the improvement of the aerodynamic efficiency of a NACA 0012 and a NREL S809 is analysed through the implementation of an optimized slot as a passive boundary layer control method. A literature review was performed to establish the most optimal slot characteristics before its implementation into the airfoils. The airfoils were constructed, and experimental tests were conducted in the University of Bristol wind tunnel at a chord-based Reynold's number of $\mathbf{2.\ 87x10^5}$***. The aerodynamic forces generated by the slotted airfoils and their respective baseline unslotted configurations were obtained through an ATI force balance system. The slotted and unslotted NACA 0012 was studied from*** $a = 0º$ ***to*** $a = 18º$ ***and the slotted and unslotted NREL S809 was examined from*** $a = 0º$ ***to*** $a = 20º$ ***. The lift and drag coefficients as well as the lift-to-drag ratio were compared for the different airfoil configurations. Particle Imaging Velocimetry analysis was also performed utilizing a LaVision laser to determine the velocity and the vorticity of the airflow around the studied airfoil and examine if the slot inclusion reduces the flow separation. The results show that the slot improves the aerodynamic efficiency of the airfoil at all angles of attack and although a drag penalty is observed at high angles of attack, the slotted airfoil provides an increased lift coefficient for all of them.***

Keywords: *NACA 0012, NREL S809,* Slot, Wind tunnel, PIV

Nomenclature

C_L	=	Lift Coefficient	C_D	=	Drag Coefficient
X	=	Slot Location (%)	γ	=	Slot width
ψ	=	Slot Slope	Y_1/Y_2	=	Slot Section Ratio
l	=	Airfoil chord length	V	=	Airspeed Velocity
ρ	=	Density of the air	S	=	Span of airfoil
L	=	Lift Force	D	=	Drag Force
α	=	Angle of Attack	μ	=	Kinematic viscosity of air

Supervised by Dr. Mark Gilbertson

Department of Mechanical Engineering

University of Bristol 2022

DECLARATION

This project report is submitted towards an application for a degree in Mechanical Engineering at the University of Bristol. The report is based upon independent work by the candidate. All contributions from others have been acknowledged and the supervisor is identified on the front page. The views expressed within the report are those of the author and not of the University of Bristol.

I hereby assert my right to be identified as the author of this report. I give permission to the University of Bristol Library to add this report to its stock and to make it available for consultation in the library, and for inter-library lending for use in another library. It may be copied in full or in part for any bone fide library or research worker on the understanding that users are made aware of their obligations under copyright legislation.

I hereby declare that the above statements are true.

1 INTRODUCTION

Is it possible to optimize the operation of wind turbine rotors by employing slotted airfoils? This question compiles the motivation of many researchers to obtain a large quantity of wind power with a high aerodynamic efficiency in wind turbines.

The urge for the increase in clean energy sources due to the devastating effects caused by the burning of fossil fuels has incremented significantly over the past years. In many countries, the implementation of wind energy for the generation of electricity has become a highly feasible option, as it offers the lowest cost alternative for the power plants being installed, encouraging researchers to develop efficient wind turbines systems that achieve the maximum attainable quantity of wind power.

Even with the influence of *COVID-19*, 2020 set a record for the wind energy industry, attaining $93GW$ of global wind power, signifying a 53% increase with respect to the previous year, according to *GWEC* [1] . This drives the total global wind power capacity up to $743\ GW$, preventing the release of over 1.1 billion tonnes of carbon dioxide. However, further efforts must be adopted if the net zero target is to be met by 2050, tripling the wind power installation rate throughout the next decade to avoid the catastrophic consequences of climate change.

1.1 Literature Review

From an aerodynamic point of view, according to *Y.P. Ju and C.H. Zhang* [2] an advantageous wind turbine airfoil must present the following characteristics:

- High C_L and high C_L/C_D ratio when operating.
- Favourable behaviour during the random and uncertain action of wind.
- Low response to the roughness of the leading edge.

Despite the abundant research performed by many researchers including *Bizzarrini et al*. [3], F. *Grasso* [4], *Li et al.* [5], or *Sagol et al* [6] to develop an optimized airfoil that satisfies the three presented characteristics, an airfoil design that meets these requirements is difficult to develop due to the airfoil not displaying these characteristics throughout the whole operational regime of wind. The value of the C_{Lmax} obtained, as well as the angle of attack at which the undesirable stall conditions arise in the wind turbine airfoil are strongly influenced by the viscous effects in the boundary layer, which is the flow immediately adjacent to the surface of the airfoil. The detachment of the boundary layer from the airfoil causes stall. Stall generates a sudden decrease in the lift of the airfoil, reducing the aerodynamic efficiency and therefore increasing the power losses. A value that quantifies the aerodynamic efficiency of an airfoil is the C_L/C_D ratio, and therefore an airfoil that achieves high value of this quantity is desired. The increase of the C_L/C_D ratio can be achieved through the passive or active control of flow separation. Contrary to active flow control, passive control does not need any energy expense, as no auxiliary power is required.

An example of passive control for regulating flow separation is the inclusion of vortex generators in the airfoil. *G. Godard* [7] investigated this by introducing vortex generators of different shapes in an airfoil. He then examined the boundary layer separation at high angles of attack employing hot wire anemometry and PIV analysis. The results displayed how the inclusion of triangular vortex generators reduced 20% the skin friction drag experienced by the airfoil when compared to a baseline airfoil where no vortex generators were introduced. This drag reduction increased the aerodynamic efficiency of the airfoil and therefore delayed stall conditions. Other researchers attempted to increase the aerodynamic performance of the airfoil through passive flow control by introducing a gurney flap. This consists of a trailing edge tab placed perpendicular to the pressure side of the airfoil that increases the C_L attained by the airfoil. According to [8], Dane Gurney was the discoverer of this device.

The establishment of a slotted airfoil to improve the stall prediction of wind turbine airfoils by passive control was first investigated by *Weick* [9] , where various slot positions and thicknesses were analysed to determine what arrangement gives the maximum aerodynamic efficiency. This was further studied by *M.Ramzi* and *G.AbdErrhmane* [10] who, by performing a 2D study on a slotted airfoil in a compressor cascade, discovered that a reduction of 28.3% in the loss coefficient can be achieved if the slot is placed at the midpoint of the separation and the minimum pressure point.

1.2 Aerospace Applications

Due to the objective of acquiring an optimized slotted airfoil configuration that allows a higher aerodynamic efficiency to attain minimized power losses in wind rotors, many researchers from the aerospace sector seek to introduce slotted airfoils into rotorcraft. The necessity for rotorcrafts that exhibit a higher endurance and flight velocity in addition to admitting an increased payload capacity is essential when designing the next generation of rotorcraft. However, these characteristics cannot be satisfied with the fixed, single-element airfoil currently being implemented.

The investigation performed by *W.Noonan* [11] revealed an increment in the lift coefficient achieved when studying a RC(6)-08 slotted rotorcraft airfoil in a transonic pressure tunnel, with varying Reynolds number from $4.1x10^6$ to $9.0\ x10^6$. During this study, a slotted airfoil was employed. This slotted airfoil allowed the movement of high-pressure airflow from the bottom side of the airfoil to the upper side, re-energizing the boundary layer and delaying stall conditions. This resulted in a $29\% - 61\%$ increase of the C_{Lmax} in the slotted RC(6)-08 airfoil in comparison to the unslotted *NACA 0012*.

A3c slotted airfoils have been implemented into a UH-60A helicopter in a CFD analysis [12]. The application of this slotted airfoil resulted in a 25% increase in the lift force and an increase in the manoeuvring effectiveness experienced by the helicopter, in comparison to when an unslotted *C106* airfoil was used.

1.3 Motivations and Objectives

The increasing need for obtaining reduced power losses in current wind turbines requires wind turbine airfoils to be re-designed to enhance their aerodynamic performance. The aerodynamic performance is highly influenced by the drag force generated by the airfoil, which sharply increases when there is a detachment of the boundary layer. Therefore, airfoils must be constructed so that they provide a maximized aerodynamic efficiency throughout their operation. The obtention of this optimized airfoil design is crucial, as it will mean a reduction in the environmental impact as well as in the operational cost of turbines.

Taking this into account, the principal objective of this research project is to analyse the detachment of the boundary layer in two types of airfoils: *NACA 0012* and *NREL S809*. The aerodynamic efficiency is analysed for a baseline unslotted *NACA 0012* airfoil and compared to the aerodynamic efficiency of a slotted *NACA 0012*. Similarly, the results obtained for an unslotted *NREL S809* wind turbine airfoil are compared to when a slotted *NREL S809* is utilized. This airfoil was selected as it was particularly designed for Horizontal Axis Wind Turbines (HAWT) applications. Despite the difficulties regarding the installation and transportation that these wind turbines present, they display a series of advantages when comparing them to other types of wind turbines such as the ones carrying a vertical axis [13]. For instance, HAWT offer a high energy output of 6 million kWh/*year* on average, which is sufficient to supply electricity to 1500 EU average households.

The four airfoils will be analysed at various angles of attack and the airflow around the airfoils will be examined making use of Particle Image Velocimetry, which captures the instantaneous velocity of the fluid around the airfoil, tracking the direction of motion of surrounding particles and therefore computing an image of the overall airflow. In contrast to other methods, this technique can

determine the strain and vorticity of the flow surrounding the airfoil, offering a graphical representation of it.

The angle of attack at which the maximum aerodynamic efficiency is achieved for the slotted airfoils will be determined, as this will result in a reduction in the power losses for the wind rotor and will offer an increase in the aerodynamic efficiency.

2 METHODOLOGY

2.1 Airfoil Description

The unslotted *NACA 0012*, slotted *NACA 0012* and slotted *NREL S809* were constructed by the *Faculty of Engineering Technical Services Workshop*. The precision of the manufactured airfoils was assessed by comparing the constructed airfoils to the models performed using the *Solidworks* software. The three airfoils had a span of 450 *mm* and a chord length of 150 *mm*.

The *SolidWorks* design of the baseline unslotted *NACA 0012* airfoil as well as the design for the slotted *NACA 0012* airfoil are displayed in Figure 1. These airfoils have a maximum thickness of 12% located at 30% of the chord from the leading edge and it have no camber. Both airfoils were constructed, and the criteria considered to determine the characteristics of the implemented slot in the slotted *NACA 0012* are described in the following section.

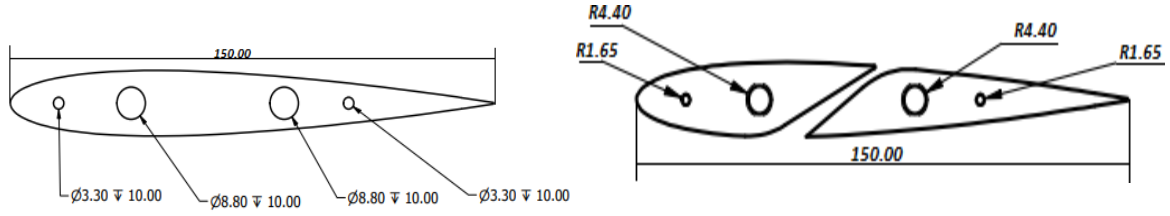

(1a) *(1b)*

Figure 1: SolidWorks Computer Aided Designs for (a) the baseline unslotted NACA 0012 airfoil and (b) slotted NACA 0012 airfoil.

The *SolidWorks* design of the baseline unslotted *NREL S809* airfoil as well as the design for the slotted *NREL S809* airfoil are displayed in Figure 2. This airfoil has a maximum thickness of 21% . Although the design of the unslotted *NREL S809* was computed, this airfoil was not manufactured by the *Faculty of Engineering Technical Services Workshop*. However, the slotted *NREL S809* was constructed.

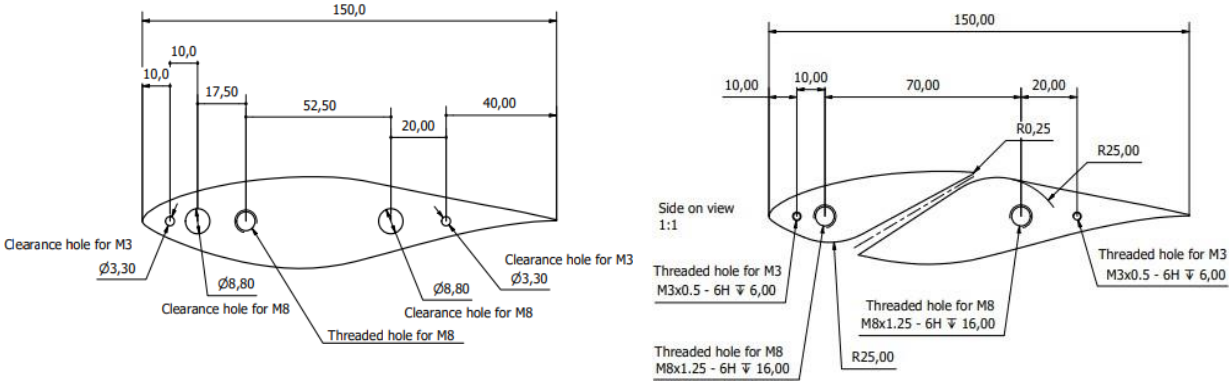

(2a) *(2b)*

Figure 2: SolidWorks Computer Aided Designs for (a) the baseline unslotted NREL S809 airfoil and (b) slotted NREL S809 airfoil.

2.1.1 Slot Geometry

The geometry of the slot had to be meticulously studied before its implementation into the slotted *NACA 0012* and slotted *NREL S809* airfoils for the assessment of their aerodynamic performance as a passive boundary layer control method. The geometric requirements for the development of the slot are displayed in Figure 3. These requirements were determined after performing an analysis of which slot characteristics offered the greatest aerodynamic performance.

To determine the most advantagoeus slot location (X), slot width (γ), slot slope (ψ) and slot section ratio (Y_1/Y_2) , the investigation performed by *R.Belamadi et al* was utilized [14]. During this investigation, a baseline unslotted *NREL S809* airfoil was altered employing a CFD simulation where a two-diemnsional numerical analysis was perfromed to determine the most effective slot characteristics. A standard $k - \varepsilon$ turbulence model was employed during their investigation as this model offered the best compromise between having a low computational error and presicion in the results obtained.

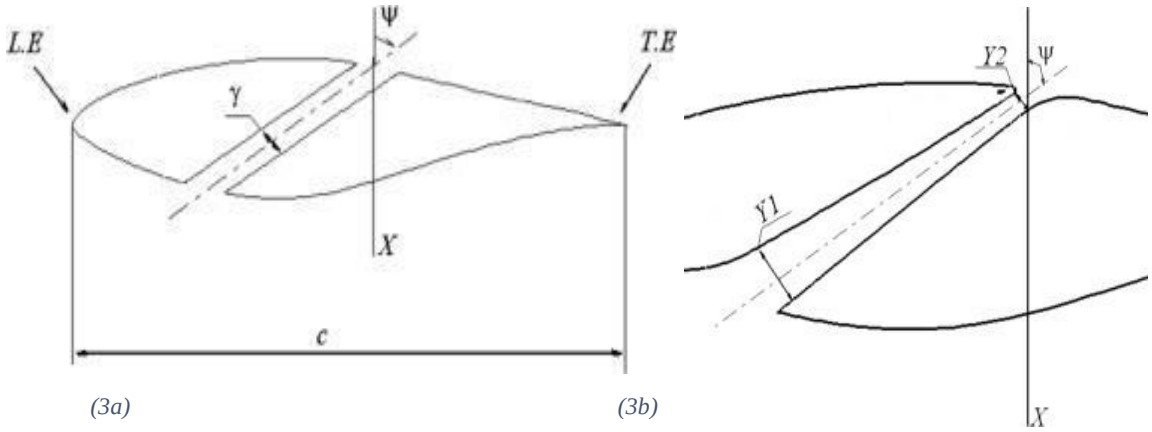

Figure 3: (a) Parameters of the implemented slot and (b) close-up of the final slot configuration implemented into the slotted NACA 0012 and slotted NREL S809 [14]

The aerodynamic efficiency of the slotted airfoil is influenced by the location at which the slot is positioned (X). In the parametric study performed by *R.Belamadi et al* [14], the glide ratio Cl/Cd was analyzed for ten slot loactions at various angles of attack. The results obtained displayed that the maximum lift coefficient was obtained when the slot was located at $X = 50\%$ and $X = 60\%$ for all angles of attack. However, the increase in the lift coeffcient for the slotted *NREL S809* compared to the baseline case was more pronounced at higher angles of attack. Therefore, the presence of the slot in these positions contributes positively to the boundary layer control, especially at high angles of attack. Slot locations below 40% did not result in an improved aerodynamic efficiency due to the fluid flowing through the slot from the pressure side not possesing enough kinetic energy to re-energize the boundary layer at the suction side. Similarly, slot locations larger than 60% aumengted the boundary layer separation.

The ratio between the width at the inlet of the slot to the width at the outlet of the slot (Y_1/Y_2) has a repercussion over the aerodynamic efficiency the wind turbine airfoil displays. This is due to the velocity of the incoming flow from the pressure side being influenced by this ratio. In investigation [10], the boundary layer separation was assessed for the slope ratios of $Y_1/Y_2 = 2, Y_1/Y_2 = 3$ and

$Y_1/Y_2 = 4$. It was found that the separation of the boundary layer was eradicated with a ratio of $Y_1/Y_2 = 4$, which offered an improvement of 32.3% in the glide ratio compared to the baseline non-slotted case. This indicates that when the speed of the flow at the outlet of the slot is increased, the aerodynamic performance is enhanced.

Likewise, the impact of the slope of the slope (ψ) on the glide ratios was assessed by *R.Belamadi et al* by setting the slot position at $X = 50\%$. The gathered data displayed a greather reduction of the flow separation when a slope of $\psi = -60º$ was employed, where an increase of *20.9%* in the glide ratio was attained when compared to the baseline configuration.

After conducting detailed research of the optimal slot parameters, it has been concluded that the most advantageous aerodynamic performance of an airfoil is achieved when $Y_1/Y_2 = 4, X = 50\%$ and $\psi = -60º$. Consequently, this slot configuration demonstrates the greatest impact for passive boundary layer control. As a result, these values were the ones employed for the manufacture of the slotted *NREL S809* and the slotted *NACA 0012* utilized in this research project.

2.2 Wind Tunnel Setup

The aerodynamic performance of the unslotted *NACA 0012*, slotted *NACA 0012* and slotted *NREL S809* was evaluated in a low turbulence wind tunnel at the *University of Bristol*. This wind tunnel constructed by *Dr R. V. Barret* [15] was designed to display a reduced turbulence intensity of 0.05%. The working section displays an octagonal shape with dimensions of $0.6m \ x \ 0.8m$ and a length of $1.6m$. The airflow can achieve a velocity up to $100m/s$ inside the testing region of the wind tunnel. The wind tunnel is equipped with an ATI force balance system and, during the testing in the wind tunnel, this balance was utilized for the obtention of precise measurements regarding the aerodynamic loads experienced by the airfoils.

The three manufactured airfoils were mounted into the wind tunnel through their aerodynamic centre (situated at the quarter chord) by means of a strut. This strut supports the airfoil inside the working section, avoiding any arising vibrations caused by the operational wind tunnel, and transmits the aerodynamic forces experienced by the wing models to a loadcell. As the loadcell is connected to a Data Acquisition (DAQ) System, the lift forces (measured in the z-axis) and drag forces (measured in the x-axis) are transferred to a computer.

This way, the aerodynamic forces experienced by the three airfoils were determined. During the research project, the wind tunnel airspeed was set to $25 \ m/s$ and the chord-based Reynold's number was established to be $2.87x10^5$. For this calculation, the air inside the wind tunnel is assumed to be incompressible, having a constant density $\rho = 1.225 \ kg/m^3$ and a constant kinematic viscosity of $\mu = 1.6x10^{-5} \ m^2/s$.

The aerodynamic forces on the unslotted and slotted *NACA 0012* were evaluated at angles of attack $0º$ to $18º$ whereas the slotted *NREL S809* was also evaluated at $20º$. This is because stall conditions still did not occur at $18º$. To change the angle of attack of the airfoils, a digital inclinometer was employed which enabled the airfoils to be set at the desired angles of attack at an accuracy of $0.2º$.

Once the lift and drag forces were obtained for each airfoil, the lift and drag coefficients were calculated, as these parameters quantify the aerodynamic efficiency of the airfoils. The variations of these coefficients with increasing angles of attack were evaluated to identify the angle of attack that provides a maximized C_L and a minimised C_D. The angle at which the detachment of the boundary layer takes place causing stall conditions was also determined.

Due to the antagonistic objectives in minimizing the drag coefficient while maximizing the lift coefficient, the glide ratio, C_L/C_D, is the selected parameter to assess whether the implementation of a slot in the *NREL S809* and *NACA 0012* airfoil offers an improved performance over their corresponding baseline unslotted airfoils. Therefore, the variation of the glide ratio with increasing angles of attack was also computed.

2.3 Particle Imaging Velocimetry

Once the aerodynamic forces of each airfoil were measured, the behaviour of the airflow around the airfoils for different angles of attack at an airspeed velocity of $25\ m/s$ was computed employing PIV. This is a flow visualization technique which displays quantitatively the instantaneous velocity field of particles in the flow field surrounding the airfoil, by tracking the motion of the particle along the testing region of the wind tunnel. Unlike other methods, PIV provides a physical understanding of the entire airflow behaviour around the airfoil and simplifies the extraction of data as well as the visualization of results.

A standard *LaVision* stereo PIV laser [16] was utilized for this experiment where an *Nd:YAG* laser generating $500\ mJ$ per pulse at a nominal pulse frequency of $12.5\ Hz$ is employed. For the application of this technique, the testing area was seeded and filled with neutrally buoyant oil particles of minuscule diameter to guarantee a sharp scattering behaviour of light and ensure their detection. When an abundant level of seeding was reached, the double pulsed laser was directed towards airfoil under investigation and so the surrounding airflow particles were targeted twice by the laser beam. Each pulse had a duration of $5ns$. The airfoils had to be coated with matte black paint to ensure the correct reflection of the laser on the surface of the airfoil.

A charge-coupled device camera was placed perpendicular to the airfoil to capture the scattering of light that the seeding particles produced. Due to the double pulse laser, two images were computed, one for each laser pulse. The temporal windows between the images obtained was $1ns$ to ensure that the particles are precisely tracked. With this, the position of the particles at these two instances was registered. The setup of this procedure can be seen in Figure 4.

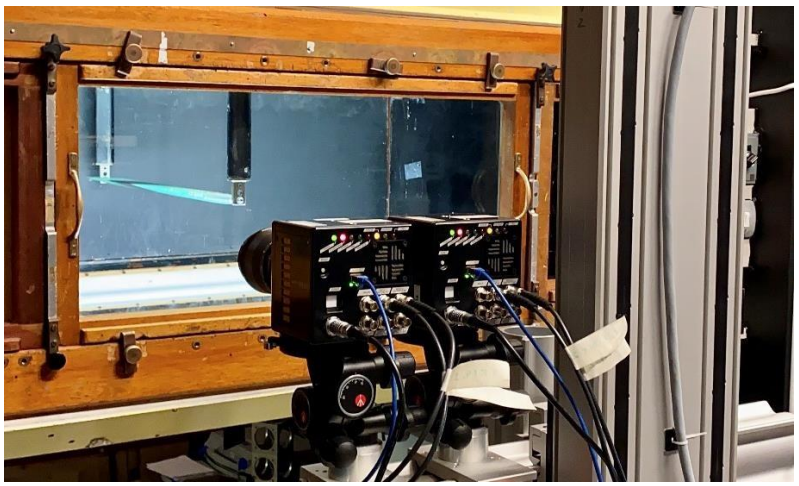

Figure 4: Experimental setup for the PIV measurements in the wind tunnel at University of Bristol

The *DaVis* and *LaVision* software was utilized to gather the recorder data and, in the end, a time evolution of the flow around the airfoils was acquired. For each angle of attack, 4000 time steps were obtained, each time step containing $29{,}928$ points with the xy coordinates of the seeding particles. The gathered data included information regarding the velocity of the seeding particles in the x and y direction as well as their vorticity.

For the purpose of analysing the entire flow field, the time average for the 4000 time steps was computed employing *MATLAB* for each angle of attack. With this, the average velocity magnitude of the airflow and the average vorticity were calculated for each airfoil at each angle of attack.

3 RESULTS AND DISCUSSIONS

3.1 Aerodynamic Forces

The key to understand the aerodynamics of an airfoil is to comprehend the force experienced by the airfoil. When the flow encounters the leading edge of an airfoil, it experiences an increase in its velocity as it goes through the suction side (upper region) of the airfoil. This increase in velocity appears simultaneously with a decrease in the static pressure of the flow, generating a pressure gradient between the suction side and the pressure side of the airfoil. This pressure gradient between the pressure side and the suction side of the airfoil generates a net turning of the airflow. Due to Newton's third law, this tuning motion of the airflow will generate an upwards force perpendicular to the direction of the wind encountering the airfoil, known as lift force. This lift force appears at the expense of drag.

Experimental curves for the comparison of the aerodynamic performance between slotted *NACA 0012* and the unslotted *NACA 0012* as well as the slotted *NREL S809* with the unslotted *NREL S809* are presented below at $Re = 2.87x10^5$. To assess the aerodynamic performance of the airfoils, the lift coefficient and drag coefficient for each airfoil were calculated by $C_L = 2L/\rho V^2 S$ and $C_D = 2D/\rho V^2 S$ employing the lift and drag forces obtained in the wind tunnel test at each angle of attack. Note that, the C_L and C_D at each angle of attack for the unslotted *NREL S809* were obtained from literature [17] as this airfoil was not constructed and could not be evaluated inside the wind tunnel.

The maximum C_L occurring just before the stalling angle is accompanied by an increment in the induced drag, so C_L,and C_D must be considered simulatneously. Therefore, to analyse the aerodynamic efficiency of the slotted airfoils in contrast to the baseline unslotted cases, the C_L/C_D ratio is computed for increasing angles of attack.

3.1.1 NACA 0012

The unslotted *NACA 0012* and slotted *NACA 0012* airfoil was mounted into the testing region of the wind tunnel and the aerodynamic forces obtained at angles of attack from $\alpha = 0º$ to $\alpha = 18º$ were obtained at an airspeed velocity of 25 m/s. The lift and drag coefficients were calculated and their evolution with increasing angles of attack is displayed in Figure 5.

In both airfoils, the lift coefficient linearly increases with the angle of attack until stall conditions are reached. At this point, there is a reduction in the lift force while the drag force increases sharply so the boundary layer will be detached, and the airflow will not follow the contour of the upper surface of the airfoil. The angle of attack at which stall conditions appear for the slotted *NACA 0012* is $\alpha = 12º$, whereas for the baseline case this critical angle occurs at $\alpha = 10º$. Therefore, it is visible in Figure 5a that the presence of the slot allows the airfoil to achieve higher C_L at all angles of attack, generating greater lift forces. The C_{Lmax} attained by the slotted *NACA 0012* is 0.753 compared to 0.561 achieved by the baseline case, accounting for a 34.5% increase in the C_{Lmax} when the slot is included. Although the slot inclusion generates more drag forces than the baseline case, Figure 5a displays how the maximum difference between the drag coefficients are 46.7% at an angle of $\alpha = 18º$. However, at this angle of attack stall conditions have already been reached and therefore the airfoils will not operate at this angle. Prior to stall, the differences between the drag coefficients are minimum and so it is concluded that the slot generates an increased lift force without producing additional drag.

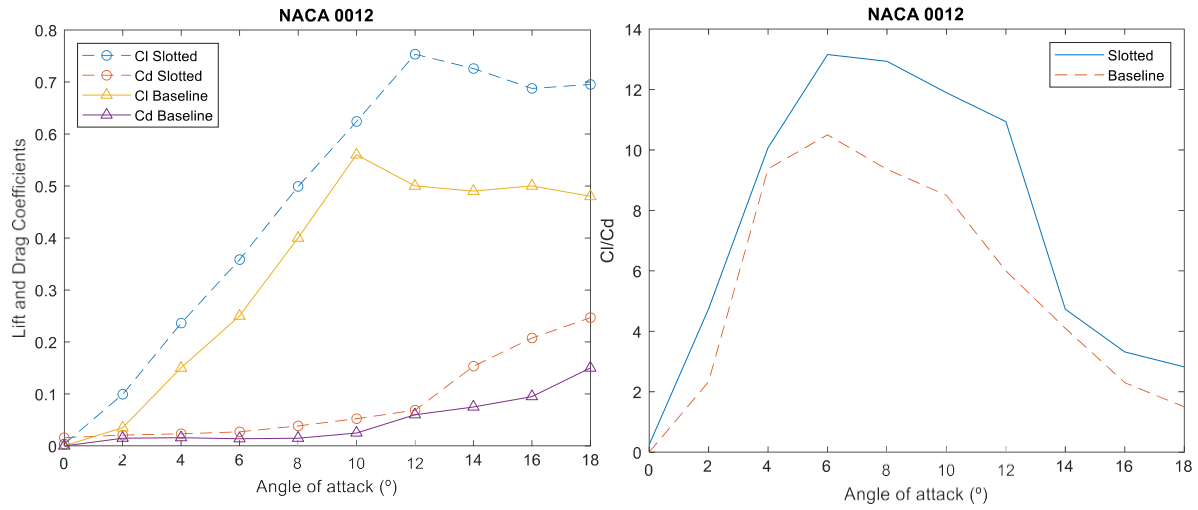

(5a) *(5b)*

Figure 5:Graph (5a) displaying how Cl and Cd varies with the angle of attack and (5b)how the Cl/Cd ratio varies with the angle of attack for the unslotted and slotted NACA 0012

The most efficient angle of attack for the slotted *NACA 0012* can be found by taking the maximum point on the C_L/C_D curve displayed in Figure 5b. This curve shows how the most efficient angle for the slotted *NACA 0012* is $\alpha = 8º$ as opposed to the baseline case where the most efficient angle occurs at $\alpha = 6º$. These angles are where each airfoil exhibit the highest lift force for the lowest drag force. Also, the maximum C_L/C_D ratio achieved by the slotted *NACA 0012* is 23.1% higher than the one attained by the baseline case. Consequently, the slotted *NACA 0012* improves the aerodynamic performance of the airfoil and will present a reduction in the power losses when operating in wind turbines or in related applications.

3.1.2 NREL S809

Similarly, the slotted *NREL S809* airfoil was mounted into the testing region of the wind tunnel and the aerodynamic forces obtained at angles of attack from $\alpha = 0º$ to $\alpha = 20º$ were obtained at an airspeed velocity of $25\ m/s$. Unlike the previous experiment, the investigation of *NREL S809* was extended until $\alpha = 20º$ because the lift force was still in augmentation at $\alpha = 18º$, meaning that stall conditions were not yet achieved. The lift and drag coefficients were calculated for the slotted *NREL S809* and for the unslotted *NREL S809* these coefficients were obtained from [17]. The evolution of these with increasing angles of attack is displayed in Figure 6.

Figure 6a illustrates how with the slotted *NREL S809* stall conditions occur at $\alpha = 18º$. This shows how the inclusion of a slot in *NREL S809* delays the boundary layer detachment as this phenomenon occurs at $\alpha = 14º$ for the baseline case unslotted *NREL S809*.

In addition to this, the C_{Lmax} achieved when employing the *NREL S809* is 1.19 which is 32.2% higher than the C_{Lmax} for the unslotted *NREL S809* and 58.0% higher than the C_{Lmax} for the slotted *NACA 0012*. This demonstrates that the presence of slot accompanied by the implementation of a cambered airfoil significantly increases the lift force. This is because the 21% thickness introduced in the *NREL S809* will generate an increase in the differential change in the momentum of the surrounding airflow, producing a higher-pressure difference between the pressure side and the suction side of the airfoil, resulting in an increased lift force. Also, the differences between the C_D of both airfoils are minimum for low angles of attacks. However, at high angles of attack (from $\alpha = 14º$) the additional lift generated by the slot appears at the expense of drag and so C_D for the slotted *NREL S809* is 25% higher than the C_D for the baseline airfoil at $\alpha = 20º$.

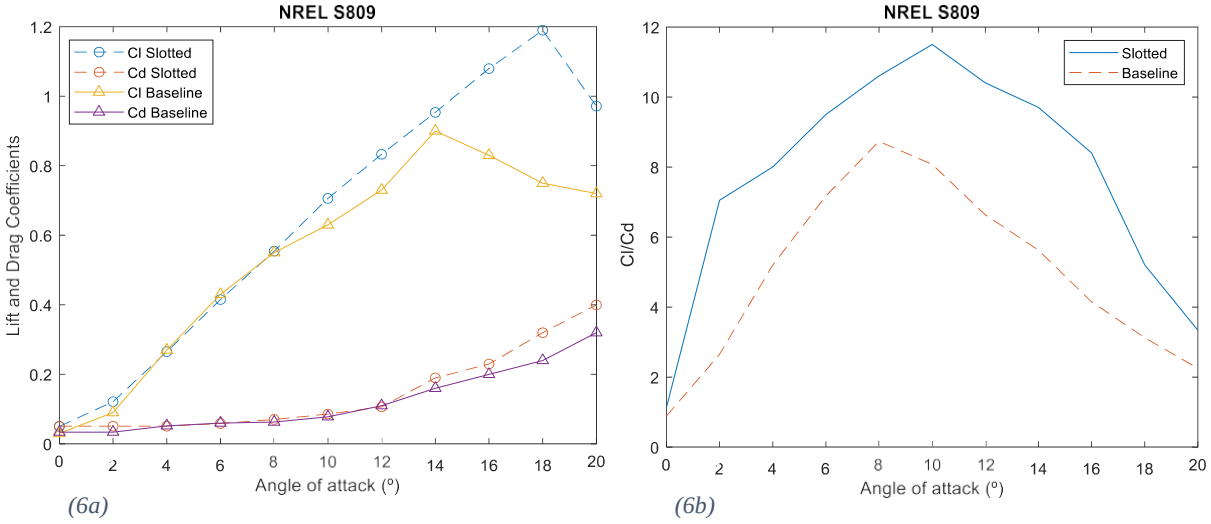

Figure 6:Graph (6a) displaying how Cl and Cd varies with the angle of attack and (6b)how the Cl/Cd ratio varies with the angle of attack for the unslotted and slotted NREL S809

The aerodynamic efficiency of the *NREL S809* mut be assessed. It can be inferred from Figure 6b that the maximum aerodynamic efficiency displayed by *NREL S809* is 11.5. This value is 31.7% higher than the one attained by the baseline case. Moreover, the angle at which this maximum C_L/C_D value is achieved increases with the slotted *NREL S809* . This is because, the most efficient angle is $\alpha = 10º$ in this airfoil, which differs from the baseline case where the most efficient angle were found to be at $\alpha = 8º$. As a result, the application of this slotted *NREL S809* airfoil into a wind turbine will allow the obtention of higher angles of attack, increasing the manoeuvring ability of the airfoil. Therefore, the airfoil will be capable to respond successfully to the stochastic behaviour of the wind without reaching stall conditions, increasing the power generation.

It is demonstrated that operating with an airfoil that includes a slot, increases the aerodynamic performance in comparison to the baseline case. The slotted *NACA 0012* presented an increase in the C_{Lmax} and in the maximum C_L/C_D ratio of 34.5% and 23.1% from its baseline unslotted airfoil, while this increase was of and 32.2% and 31.7% with the slotted *NREL S809*. In both cases, the inclusion of a slot significantly improves the aerodynamic performance of the airfoil.

3.2 PIV Results

The magnitude of the velocity and the vorticity of the airflow will be presented for the slotted *NACA 0012* and slotted *NREL S809* and compared to their baseline cases. The angles at which the PIV measurements are displayed were selected based on the most interesting points displayed on the results obtained from the aerodynamic forces.

For the clarification of visualized results, the contour of the airfoils are identified and drawn utilizing a black line to create a greater contrast between the studied region and the airfoil. Although the pressure side of the airfoil was also studied, only the suction side of the airfoil is presented as it is where the detachment of the boundary layer occurs.

3.2.1 NACA 0012

Regarding the symmetric baseline *NACA 0012* the results are displayed for angles $\alpha = 10º$ and $\alpha = 12º$. Although PIV results were obtained for angles between $\alpha = 0º$ and $\alpha = 18º$ These angles are selected as they display the behaviour of the airflow before stalling conditions and after stalling has occurred. Figure 7 illustrates the velocity and the vorticity of the airflow of baseline *NACA 0012* and slotted *NACA 0012* at an angle of attack of $\alpha = 10º$, to assess whether the slot introduces improvements in the airflow behaviour.

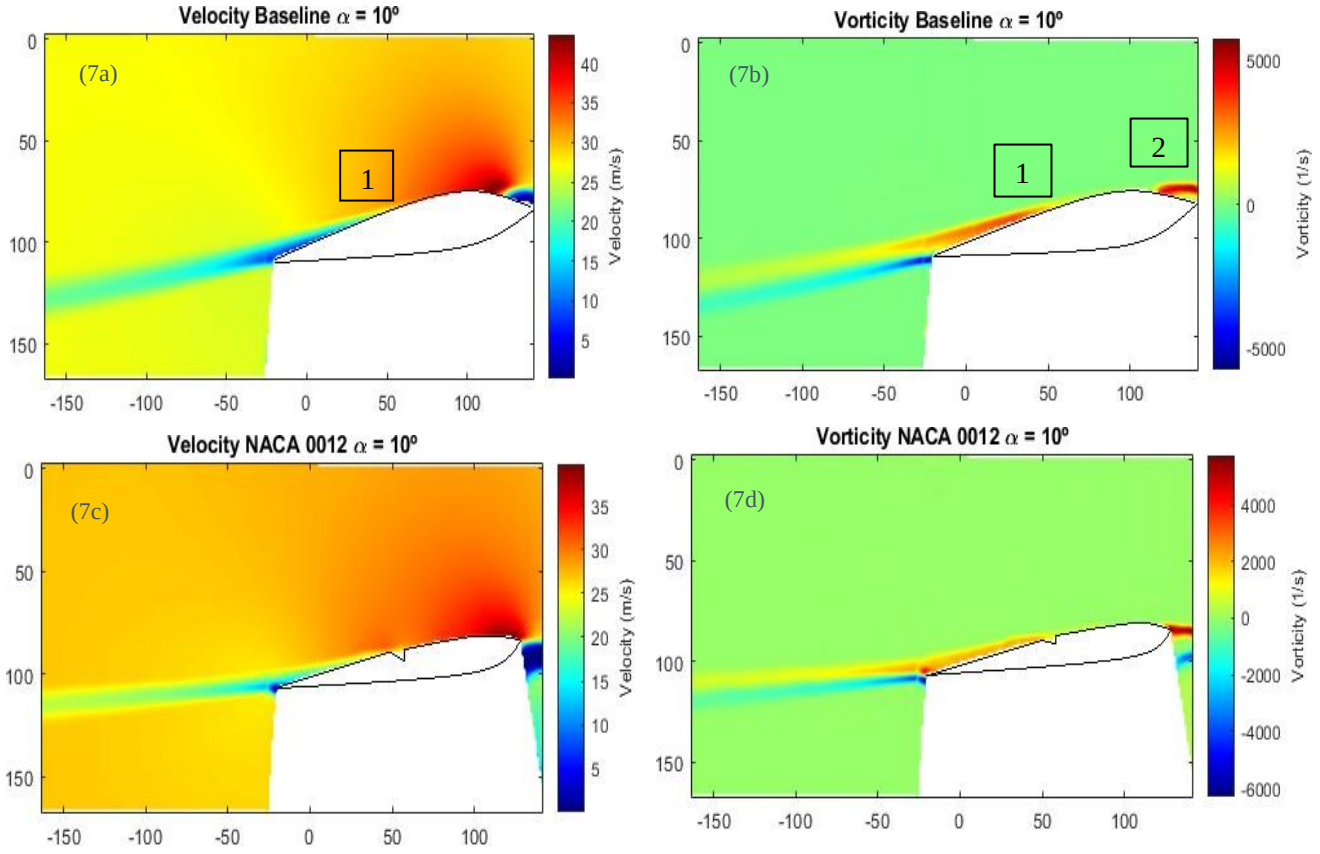

Figure 7: PIV results displaying (7a) Velocity and (7b) Vorticity of the baseline NACA 0012 and (7c) Velocity and (7d) Vorticity of the slotted NACA 0012 at 10º angle of attack.

Comparing the results obtained, the airflow in the suction side of both airfoils experience an acceleration. *Point 1* in Figure 7a shows how flow separation begins to occur in the baseline case as inferred by the increasing blue region in this figure. This is caused by the increasing vorticity arising at the same *Point 1* in Figure 7b. This figure also shows high leading edge vorticity airfoil (*Point 2*), accounting for the decrease in the velocity of the airflow at the same point in Figure 7a. This suggests that leading edge flow separation is starting to develop. This does not occur in the slotted *NACA 0012* as the blue region displayed in Figure 7c is smaller than the one displayed in Figure 7a. Therefore, the airflow leaves smoothly the trailing edge of the airfoil without generating flow separation in the slotted *NACA 0012*. Also, the vorticity generated by the slotted NACA 0012 is less than the one generated by the baseline case, generating less pressure drag.

Figure 8 displays the results obtained at $\alpha = 12º$. At this angle, there is a complete detachment of the boundary layer in the baseline case as displayed by Figure 8a, where the airflow in the suction side of the airfoil experiences an aggressive decrease in its velocity and therefore it does no longer follow the contour of the airfoil. This is caused by the wake formed due to the increase in the leading edge vorticity, which acquires values up to $6000\ 1/s$ as displayed by Figure 8b. Figure 8c shows how the airflow remains attach to the slotted *NACA 0012* at this angle of attack due to the influence of the slot and therefore no stalling conditions occur.

Moreover, it is observed that as the angle of attack increases, the velocity of the airflow in the suction side of the slotted *NACA 0012* increases, achieving values up to $45 m/s$ at $\alpha = 12º$ compared

to 37 m/s at $\alpha = 10º$. Due to Bernoulli's principle, this results in a greater pressure difference being generated between the pressure side and suction side at $\alpha = 12º$, explaining why C_{Lmax} is achieved at $\alpha = 12º$ for the slotted *NACA 0012*.

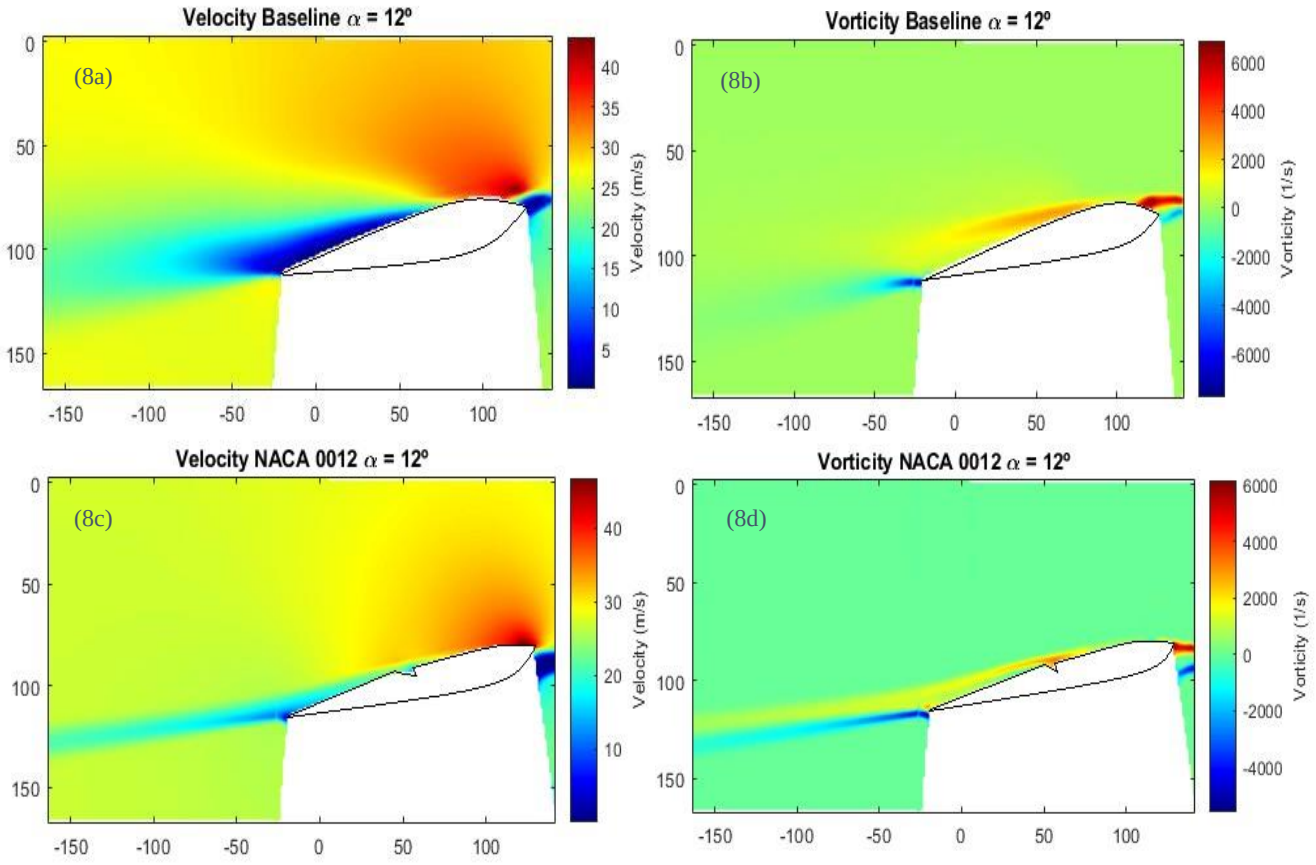

Figure 8: PIV results displaying (8a) Velocity and (8b) Vorticity of the baseline NACA 0012 and (8c) Velocity and (8d) Vorticity of the slotted NACA 0012 at 12º angle of attack

By including the slot, air containing a higher pressure flows from the pressure side to the suction side through the slot. Therefore, the slot ejects a flow carrying a high momentum into the upper surface of the airfoil which re-energizes the boundary layer, delaying the separation point and avoiding stalling conditions which would occur under the same circumstances in the unslotted airfoil. This stalling phenomenon leads to irregular oscillations arising in the airfoil provoking efficiency losses as well as power losses.

Figure 9 displays the airflow behaviour at $\alpha = 14º$ for the slotted *NACA 0012*. Figure 9a shows how leading edge flow separation occurs at this angle caused by the high vorticity generated at the leading edge due to the high angle of attack, seen in Figure 9b. Even at high angles of attack where stall has occurred, the slot can be seen to work. This is because flow is coming through the slot generating flow circulation. However, the energy contained by this fluid is insufficient to re-energize the boundary layer, as a complete strong flow separation has already occurred at the leading edge. It can be noticed how the separation point travels towards the leading edge of the airfoil as the angle of attack is increased.

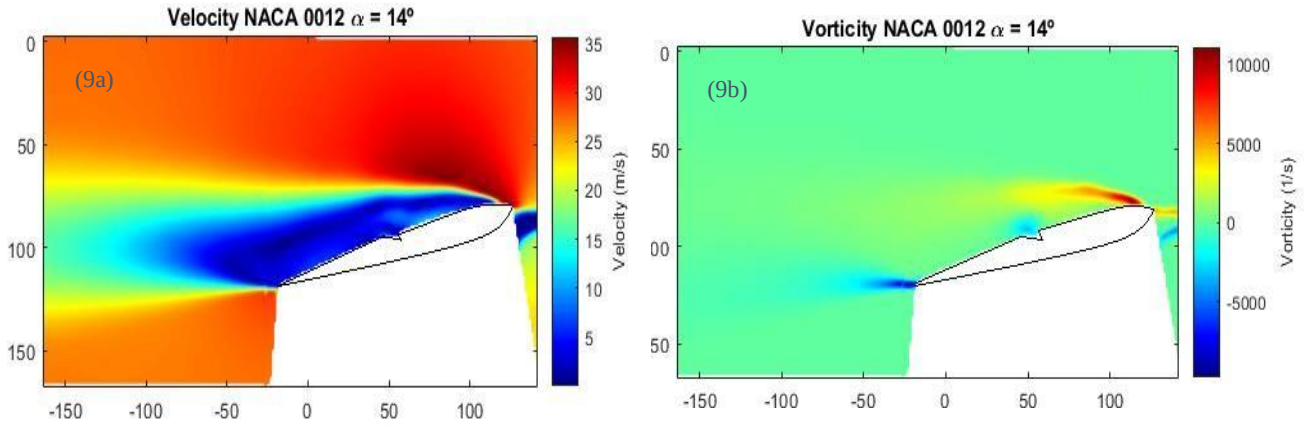

Figure 9: PIV results displaying (9a) Velocity and (9b) Vorticity of the slotted NACA 0012 at 14º angle of attack

In summary, while with the baseline airfoil the boundary layer separation occurs at $\alpha = 10º$, the inclusion of the slot delays this detachment to $\alpha = 12º$ due to the slot delivering flow from the pressure side into the suction side, supplying energy to the flow in the inner region of the boundary layer to withstand the adverse pressure gradient that causes flow separation. This allows a greater C_{Lmax} coefficient to be achieved with the slotted *NACA 0012* as well as a greater aerodynamic efficiency which will reduce the power losses when utilizing the slotted airfoil in wind turbine or in helicopter applications.

3.2.2 NREL S809

Although PIV results were obtained for the slotted *NREL S809* for $\alpha = 0º$ to $\alpha = 20º$, only the results for $\alpha = 15º$, $\alpha = 18º$ and $\alpha = 20º$ are presented. This is because, as the unslotted NREL S809 could not be constructed, the PIV results for this baseline airfoil are obtained from the investigation performed by *R.Belamadi et al.* [14] and these were the angles of attack utilized in this investigation. With this, the PIV results obtained in the wind tunnel of the *University of Bristol* for the slotted *NREL S809* are compared to the PIV results obtained by *R.Belamadi et al.* [14] for the baseline case.

Figure 10 illustrates the velocity of the airflow around baseline *NREL S809* and slotted *NREL S809* at an angle of attack of $\alpha = 15º$, to assess whether the slot introduces improvements in the airflow behaviour. The vorticity of the baseline case cannot be present due to *R.Belamadi et al.* [14] not obtaining this parameter in their investigation.

Comparing Figure 10a and Figure 10b it is seen that the baseline case produces a greater region of flow separation than the slotted case. This is because, unlike the baseline case, where more circulation of a low velocity flow is being generated, the slotted *NREL S809* shows a laminar stream of airflow leaving the trailing edge. Furthermore, Figure 10c shows how high vorticity was beginning to develop before the slot, which could have led to the detachment of the boundary layer and therefore flow separation. However, the slot is seen to introduce an injection of higher-pressure laminar air with a lower vorticity. This clearly energizes the boundary layer as the injection of this high energy airflow causes the fluid adjacent to the suction side of the airfoil to remain attached to the contour of the airfoil, preventing the separation that occurs in the baseline case under the same angle of attack.

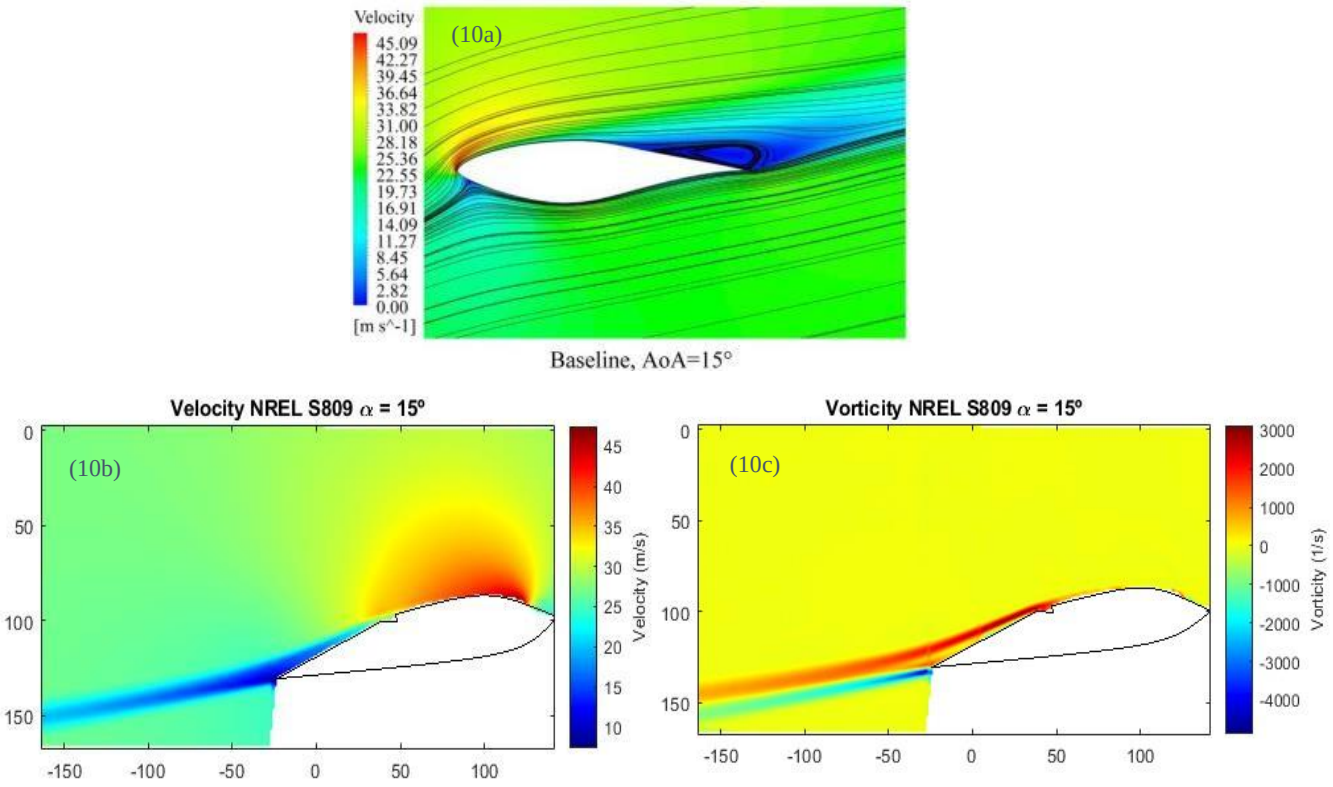

Figure 10: PIV results displaying (10) Velocity of the baseline NREL S809 obtained from [14], and (10b) Velocity and (10c) Vorticity of the slotted NREL S809 at 15° angle of attack

The benefits of the slot can be reassured by looking at Figure 11 that presents the airflow around the airfoils at $\alpha = 18º$. Figure 11a displays how the circulation of the separated flow has increased in size. This flow circulation results in the formation of eddies which decrease the flow velocity as depicted by the blue region in this figure. Unlike the baseline case, Figure 11b illustrates the absence of flow circulation and displays how the airflow remains laminar when leaving the suction side of the slotted *NREL S809*. Therefore, the slot inclusion reduces the amount of flow separation in the airfoil as well as delaying the position of the separation point. As it previously occurred at $\alpha = 15º$, Figure 11c displays how the slot introduces a higher energy airflow which is more laminar, allowing the boundary layer to remain attach by providing it with more energy to resist the adverse pressure gradient that causes stall. This figure also displays that when the angle of attack is increased from $\alpha = 15º$ to at $\alpha = 18º$, the quantity of this injected flow increases.

Moreover, at $\alpha = 18º$ more significant velocity variations are encountered than at $\alpha = 15º$, and the fluid reaches values up to $55\ m/s$ in the suction side in contrast to the $45\ m/s$ reached at $\alpha = 15º$. This means that larger pressure differences arise at $\alpha = 18º$ and therefore a greater lift force will be accomplished by the slotted *NREL S809* at this angle of attack. This explains why a greater aerodynamic efficiency was obtained at this angle of attack.

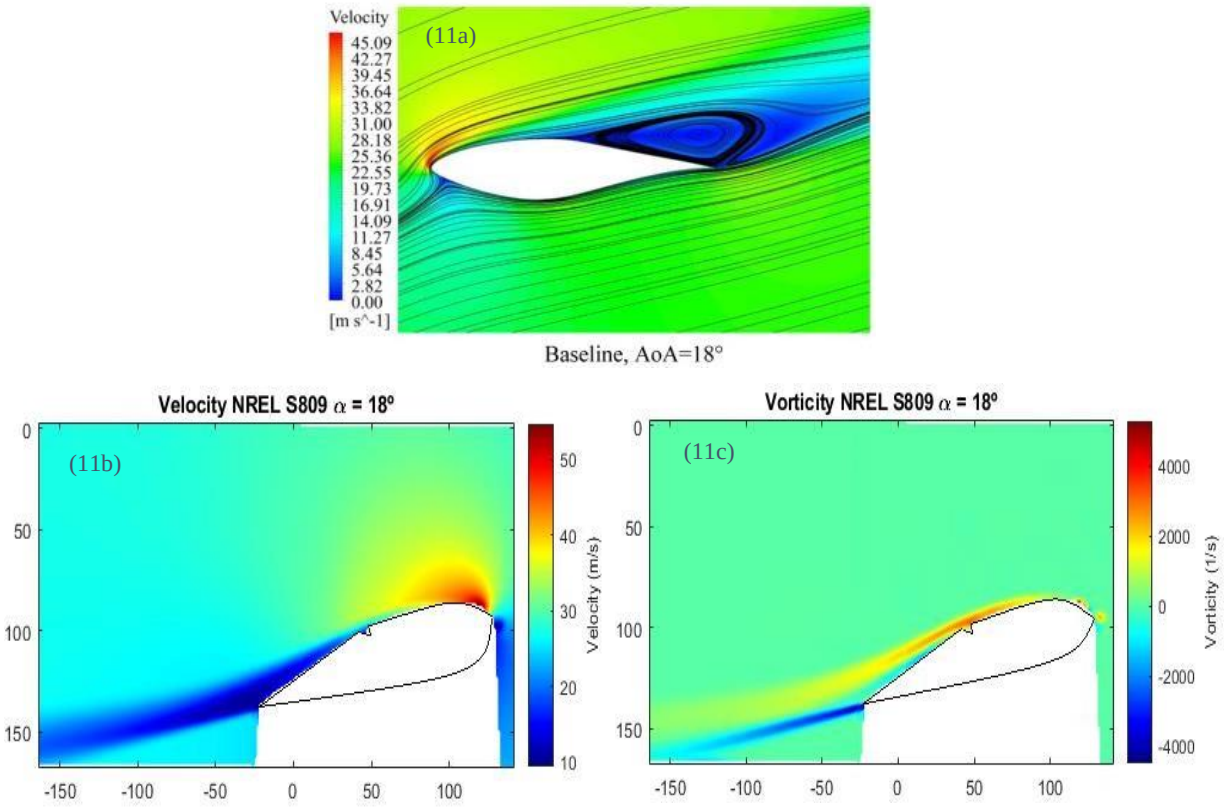

Figure 11: PIV results displaying (10) Velocity of the baseline NREL S809 obtained from [14], and (10b) Velocity and (10c) Vorticity of the slotted NREL S809 at 18º angle of attack

Analysing the results obtained $\alpha = 20º$ illustrated in Figure 12, it is observed that there is complete leading edge flow separation through the entire suction side of the airfoil. This is caused by the originating leading edge vorticity seen in Figure 12c due to the high angle of attack. This causes strong stall to occur and in both airfoils the circulation of this stall air can be seen in Figures 12a and 12b in the large blue region. Flow circulation through the slot is noticed at $\alpha = 20º$ as shown by the black arrow in Figure 12c, and this causes a secondary flow circulation to originate at the slot location. Although this flow injection is insufficient to re-attach the boundary layer, this secondary circulation is seen to improve the aerodynamic performance of the airfoil as the slotted *NREL S809* has a higher C_L/C_D value at $\alpha = 20º$ than the baseline case.

The implementation of a slot in a cambered *NREL S809* airfoil results in the delay of the boundary layer detachment. Greater angles of attacks can be achieved with the slotted *NREL S809* without stall conditions originating. This is because, complete flow separation did not start originating until $\alpha = 20º$ in contrast to the baseline case where this occurred at $\alpha = 14º$. In addition, the presented results show how the lift coefficient is maximized with the slotted *NREL S809* due to the greater velocities attained by the airflow in the suction side seen in the PIV results.

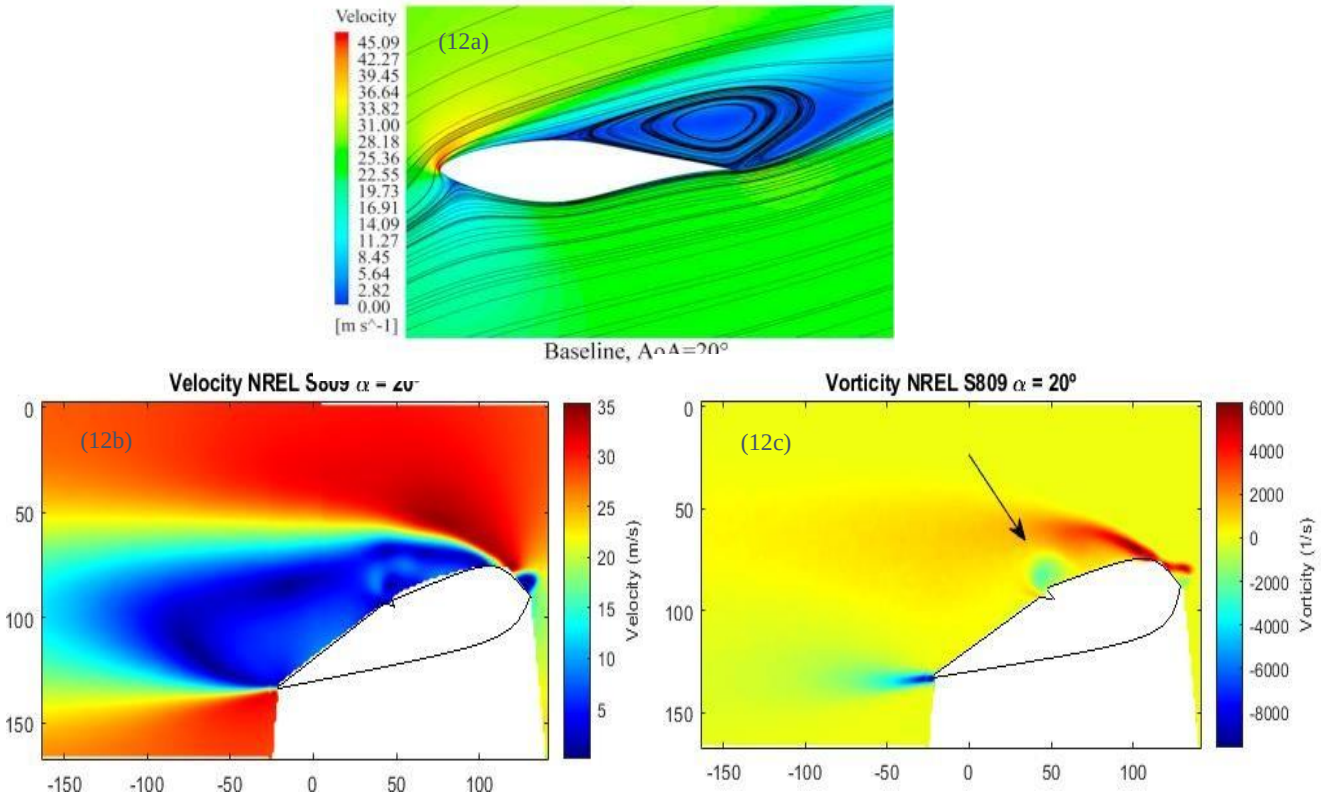

Figure 12: PIV results displaying (12a) Velocity of the baseline NREL S809 obtained from [14], and (12b) Velocity and (12c) Vorticity of the slotted NREL S809 at 20º angle of attack

In summary, the analysis of the aerodynamic forces as well as the PIV visualization displays how the slot inclusion generates a higher aerodynamic efficiency by allowing the airfoils to produce greater lift coefficients without generating a lot of drag, especially at lower angles of attack. PIV showed how by considering a slot, stall conditions are less aggressive and considerably delayed from $\alpha = 10º$ to $\alpha = 12º$ in the *NACA 0012* and from $\alpha = 14º$ to $\alpha = 18º$ in the *NREL S809*. This results in the slotted airfoils displaying an improved aerodynamic performance when compared to the unslotted airfoils.

3.2.3 UNCERTAINTY

During the research project, many possible sources of uncertainty in the experimental setup could have affected the PIV results. To begin with, uncertainty due to calibration factors when mounting the airfoils into the wind tunnel can generate some inaccuracy in the results obtained. Also, another source of uncertainty may arise when the inclinometer was employed to vary the angle of attack in the airfoils, as the precision of this instrument is of 0.2^{o}. As previously mentioned, the airfoils were covered in black mate paint to guarantee their detection with the PIV laser. The covering of the leading edge of the airfoils with this black paint was challenging to perform due to the curvature presented in this region of the airfoil. Therefore, the velocity and vorticity results at the leading edge have a greater uncertainty than the other regions and this must be taken into consideration during the discussion of the results.

4 CONCLUSION AND FUTURE WORK

The implementation of a slot in an airfoil has been proved to be successful as a passive boundary layer control method for its implementation in wind turbine rotors. The inclusion of a slot in a *NACA 0012* and *NREL S809* airfoil has been experimentally analysed in the wind tunnel of the *University of Bristol* to assess the aerodynamic performance of the airfoils and Particle Imaging Velocimetry was utilized to visualize the behaviour of the airflow around the airfoils at various angles of attack.

This analysis demonstrated that the presence of a slot in the *NACA 0012* increases the lift coefficient attained by the airfoil when comparing it to the baseline, unslotted *NACA 0012*. The C_{Lmax} and the maximum C_L/C_D ratio achieved by the slotted *NACA 0012* are 34.5% and 23.1% higher than the one achieved by the unslotted airfoil, leading to an improved aerodynamic performance. Likewise, the slotted NREL S809 presented a C_{Lmax} 32.2% higher than the one attained by the baseline case. The slotted NREL S809 demonstrated an improved aerodynamic efficiency than the baseline case at all angles of attack, achieving a maximum C_L/C_D value 31.7% greater than the unslotted case. The slot implementation produced higher C_D values than the baseline cases, especially at high angles of attack. This problem can be approached in future work by implementing a control system in the wind turbine rotor that permits aperture or closure of the slot depending on the angle of attack in which the wind strikes the airfoil.

Concerning the PIV analysis, the slot was observed to inject a laminar flow at a critical position of the suction side of the airfoil, where flow separation was beginning to originate. This high-pressure flow introduction re-energized the boundary layer and delayed the stall conditions that would otherwise arise in the unslotted airfoils. Stall conditions were postponed from $\alpha = 10º$ in the baseline NACA 0012 to $\alpha = 12º$ in the slotted *NACA 0012*. In the *NREL S809* stall conditions were delayed from $\alpha = 14º$ to $\alpha = 18º$ when the slot was considered. The slot also revealed a decrease in the arising vorticity that causes the boundary layer detachment. In addition, the PIV validated the slot operation at all angles of attack as it illustrated how the quantity of flow injection through the slot increases with increasing angle of attack.

In future work, pressure tabs can be implemented into the airfoils under investigation to examine the pressure distribution around the slotted airfoils in comparison with the baseline cases. This will provide an improved understanding of the flow conditions that lead to the detachment of the boundary layer due to the adverse pressure gradients. In addition, a Proper Orthogonal Decomposition (POD) analysis can be performed to reveal the energy contents in the eddies generated at stall by the slotted airfoils in comparison with the unslotted airfoils. This will determine the level of turbulence contained by the separated flow and how this affects the aerodynamic efficiency and power losses of the airfoils. This will permit the deep comprehension of slotted airfoils and therefore it will allow researchers to take full advantage of them when implementing slotted airfoils into wind turbines or into other aerospace applications.

ACKNOWLEDGEMENT

The author would like to thank Dr Mahdi Azarpeyvand for his continuous support throughout the project and as the wind tunnel supervisor.

5 REFERENCES

[1] G. W. E. Council, «Global Wind Report 2021,» GWEC, Brussels, 2021.

[2] JU, Y. P.; ZHANG, C. H. Multi-point robust design optimization of wind turbine airfoil under geometric uncertainty. Proceedings of the Institution of Mechanical Engineers, Part A: *Journal of Power and Energy*, 2012, vol. 226, no 2, p. 245-261.

[3] BIZZARRINI, Nadia; GRASSO, Francesco; COIRO, Domenico P. *Genetic algorithms in wind turbine airfoil design*. EWEA, EWEC2011, Bruxelles, Belgium, 2011, p. 14-17.

[4] GRASSO, Francesco. Usage of numerical optimization in wind turbine airfoil design. *Journal of Aircraft*, 2011, vol. 48, no 1, p. 248-255.

[5] LI, J. Y., et al. Aerodynamic optimization of wind turbine airfoils using response surface techniques. Proceedings of the Institution of Mechanical Engineers, Part A*: Journal of Power and Energy*, 2010, vol. 224, no 6, p. 827-838.

[6] SAGOL, Ece; REGGIO, Marcelo; ILINCA, Adrian. *Issues concerning roughness on wind turbine blades.* Renewable and sustainable energy Reviews, 2013, vol. 23, p. 514-525.

[7] GODARD, Gilles; STANISLAS, Michel. *Control of a decelerating boundary layer. Part 1: Optimization of passive vortex generators*. Aerospace Science and Technology, 2006, vol. 10, no 3, p. 181-191.

[8] HOUGHTON, Edward Lewis; CARPENTER, Peter William. *Aerodynamics for engineering students.* Elsevier, 2003.

[9] WEICK, Fred E.; SHORTAL, Joseph A. *The effect of multiple fixed slots and a trailing-edge flap on the lift and drag of a Clark Y airfoil*. 1933.7

[10] RAMZI, M.; ABDERRAHMANE, G. Passive Control via Slotted Blading in a Compressor Cascade at Stall Condition. *Journal of Applied Fluid Mechanics*, 2013, vol. 6, no 4.

[11] NOONAN, Kevin W.; ALLISON, Dennis O.; STANAWAY, Sharon. Investigation of a Slotted Rotorcraft Airfoil at Mach Numbers From 0.20 to 0.88 at Full-Scale Reynolds Numbers. En *Aeromechanics Specialists Conference—A Conference on Aerodynamics, Acoustics and Dynamics*. 1994. p. 4.5-1.

[12] YEO, Hyeonsoo; LIM, Joon W. Application of a slotted airfoil for UH-60A helicopter performance. NATIONAL AERONAUTICS AND SPACE ADMINISTRATION MOFFETT FIELD CA AMES RESEARCH CENTER, 2002.

[13] Horizontal Axis Wind Turbines (HAWT): Advantages and Disadvantages. *LUVSIDE*

[14] BELAMADI, Riyadh, et al. *Aerodynamic performance analysis of slotted airfoils for application to wind turbine blades.* Journal of wind engineering and industrial aerodynamics, 2016, vol. 151, p. 79-99.

[15] BARRETT, R. V. Design and performance of a new low turbulence wind tunnel at Bristol University. *The Aeronautical Journal*, 1984, vol. 88, no 873, p. 86-90.

[16] LaVision GmbH, Anna-Vandenhoeck-Ring 19, D-37081 Göttingen. PRODUCT MANUAL: FLOW MASTER. Item Number(s): 1105011-4.

[17] SPERA, David A. *Models of lift and drag coefficients of stalled and unstalled airfoils in wind turbines and wind tunnels*. 2008.